World Electric Vehicle Journal

MDPI

Article

Optimization Research on Energy Management Strategies and Powertrain Parameters for Plug-In Hybrid Electric Buses

Lufeng Wang [1,*], Juanying Zhou [2] and Jianyou Zhao [3]

[1] College of Intelligent Automobile Manufacturing, Shaanxi College of Communication Technology, Xi'an 710018, China
[2] College of Automotive Engineering and General Aviation, Shaanxi Vocational & Technical College, Xi'an 710038, China; zhoujy@chd.edu.cn
[3] School of Automobile, Chang'an University, Xi'an 710064, China; jyzhao@chd.edu.cn
* Correspondence: lfwang@chd.edu.cn

Abstract: The power split plug-in hybrid electric bus (PHEB) boasts the capability for concurrent decoupling of rotation speed and torque, emerging as the key technology for energy conservation. The optimization of energy management strategies (EMSs) and powertrain parameters for PHEB contributes to bolstering vehicle performance and fuel economy. This paper revolves around optimizing fuel economy in PHEBs by proposing an optimization algorithm for the combination of a multi-layer rule-based energy management strategy (MRB-EMS) and powertrain parameters, with the former incorporating intelligent algorithms alongside deterministic rules. It commences by establishing a double-planetary-gear power split model for PHEBs, followed by parameter matching for powertrain components in adherence to relevant standards. Moving on, this paper plunges into the operational modes of the PHEB and assesses the system efficiency under each mode. The MRB-EMS is devised, with the battery's State of Charge (SOC) serving as the hard constraint in the outer layer and the Charge Depletion and Charge Sustaining (CDCS) strategy forming the inner layer. To address the issue of suboptimal adaptive performance within the inner layer, an enhancement is introduced through the integration of optimization algorithms, culminating in the formulation of the enhanced MRB (MRB-II)-EMS. The fuel consumption of MRB-II-EMS and CDCS, under China City Bus Circle (CCBC) and synthetic driving cycle, decreased by 12.02% and 10.35% respectively, and the battery life loss decreased by 33.33% and 31.64%, with significant effects. Subsequent to this, a combined multi-layer powertrain optimization method based on Genetic Algorithm-Optimal Adaptive Control of Motor Efficiency-Particle Swarm Optimization (GOP) is proposed. In parallel with solving the optimal powertrain parameters, this method allows for the synchronous optimization of the Electric Driving (ED) mode and the Shutdown Charge Hold (SCH) mode within the MRB strategy. As evidenced by the results, the proposed optimization method is tailored for the EMSs and powertrain parameters. After optimization, fuel consumption was reduced by 9.04% and 18.11%, and battery life loss was decreased by 3.19% and 7.42% under the CCBC and synthetic driving cycle, which demonstrates a substantial elevation in the fuel economy and battery protection capabilities of PHEB.

Keywords: automotive engineering; plug-in hybrid electric bus (PHEB); energy management strategy; powertrain parameter optimization; system efficiency; GOP hierarchical method

Citation: Wang, L.; Zhou, J.; Zhao, J. Optimization Research on Energy Management Strategies and Powertrain Parameters for Plug-In Hybrid Electric Buses. *World Electr. Veh. J.* **2024**, *15*, 510. https://doi.org/10.3390/wevj15110510

Academic Editors: Henrique De Carvalho Pinheiro and Massimiliana Carello

Received: 14 September 2024
Revised: 16 October 2024
Accepted: 25 October 2024
Published: 7 November 2024

1. Introduction

The poor adaptability of traditional fuel vehicles to driving cycles renders their fuel economy and emission performance underperforming [1]. Investigating efficient, safe, and environmentally friendly powertrains, alongside advanced energy-saving control technologies, has emerged as the most prevalent avenue in the transportation sector to address the aforementioned issues. The powertrain of plug-in hybrid electric vehicles (PHEVs) stands among the most efficient automotive power systems, offering a viable solution to challenges like energy crises and environmental pollution [2]. Optimizing energy management

strategies (EMSs) and powertrain parameters in hybrid electric vehicles/PHEVs holds the promise of significantly boosting vehicle performance and fuel economy [3].

EMSs allocate the power or torque of each power source contingent upon the vehicle operation information as well as the vehicle power demand, manifesting a critical factor in augmenting the economy of a hybrid vehicle [4]. The research on energy management strategies and powertrain parameter optimization of plug-in hybrid buses is of great significance for improving vehicle performance and reducing energy consumption and emissions and is a hot topic in the research and development of new energy vehicle technologies.

Rule-based EMS typically hinges on expert experience or the steady-state characteristics of hybrid powertrain components to dictate mode switching and power source allocation among power sources [5]. These strategies, simple in their control approach, find extensive application in the practical control of PHEVs. Among the most successful strategies commercially deployed is the Charge Depletion and Charge Sustaining (CDCS) strategy [6,7], capitalizing on the advantages of clean and cost-effective electric energy to the utmost extent. The CDCS strategy adapts the powertrain's operating modes based on changes in the power battery's state of charge (SOC), each mode offering distinct features [8,9]. In the Charge Depletion (CD) mode, the power battery takes the lead as the main power source. As the power battery's SOC creases to a certain level, the engine ignites and takes over as the primary power source, initiating the Charge Sustaining (CS) mode. With a view to improving the control effect of the CDCS strategy, Pan et al. [10] optimized the SOC trajectory of power batteries in plug-in series hybrid electric vehicles (HEVs) using fuzzy logic. This strategy ensures the engine operates at its maximum fuel-efficiency range and is effective in preventing battery over-discharge. Liu et al. [11] segmented vehicle operation modes into CD and CS modes based on the power battery's SOC thresholds. They utilized a multi-objective genetic algorithm to optimize parameters within the CS mode. Ruan et al. [12] proposed a blended rule-based EMS by integrating the driving information with the CD strategy, resulting in a reduction of the engine startup/shutdown time. To address the efficiency oversight in hybrid powertrains in the current CDCS control strategy, a multitude of scholars have proposed schemes that factor in the efficiency adjustments of various components within the hybrid powertrain for mode switching and energy allocation in HEVs [13,14]. For instance, Wang et al. [15], targeting a parallel HEV, optimized the engine and motor output torque control for each operating mode to achieve maximum efficiency across the system. This approach effectively enhances system efficiency and overall vehicle fuel economy while ensuring prolonged powertrain component lifespan.

Commercial CDCS control strategies allow for real-time optimization with high implementation efficiency, providing a wide range of applications in passenger cars that prioritize the use of electric energy. However, public transportation features fixed operating routes and working mileage, and the strategy of prioritizing electric drive may fall short of yielding a more optimal energy ratio after feeding the electric power. Therefore, the CDCS strategy is improved and combined with other intelligent algorithms to realize the improvement and enhancement of the PHEB control effect for urban public transportation.

Hybrid powertrain parameter optimization involves, upon meeting the requirements for vehicle power performance and component capabilities in terms of system configuration and type selection, the process of optimizing the parameters of powertrain components (such as the engine, motor, battery, and coupling mechanism) with the goals of enhancing overall vehicle fuel economy and power performance. Optimizing the power parameters of hybrid powertrain systems wields a significant impact on an HEV's power, efficiency, and emissions, thereby enhancing the overall operational efficiency of the system [16,17]. Optimization of parameters in hybrid powertrains typically involves methods like orthogonal optimization algorithms, VisualDOC algorithms, and other optimization approaches.

Currently, driving cycle-based optimization and optimization algorithms are prevalent methods for hybrid powertrain parameter optimization [18]. Lei et al. [19] put forth a method to optimize the power source dimensions by using a combination of the Extra Urban Driving Cycle (EUDC) and the Highway Fuel Economy Test (HWEFT), resulting in a remarkable

optimization effect. Xue et al. [20] proposed a method to optimize HEV powertrain parameters based on the New European Driving Cycle (NEDC), for which the findings shed light on an enhancement of engine efficiency but lower matching efficiency. The Bees Algorithm, Particle Swarm Optimization (PSO) Algorithm, Genetic Algorithm (GA), and Simulated Annealing Algorithm find frequent utilization in HEV powertrain parameter optimization. Aslan et al. [21] put forward an optimization approach aiming to minimize fuel consumption and emissions by leveraging the Bees Algorithm to optimize critical powertrain parameters, accompanied by an assessment of vehicle performance using three typical driving cycles. Drallmeier et al. [22], targeting maximum fuel efficiency while satisfying critical performance requirements, harnessed the PSO algorithm to optimize powertrain component dimensions. This strategy improved fuel efficiency and reduced vehicle operational costs. Furthermore, Quan et al. [23] took power and economy as the optimization objectives. They used a GA to optimize characteristic parameters of the planetary gear and powertrain components in power-split HEVs, leading to an enhancement of overall power and economy. Nonetheless, relying solely on a single optimization algorithm raises issues such as insufficient local optimization capability, low convergence efficiency, and lengthy optimization cycles, limiting the full unleashing of PHEV's fuel-saving potential.

In light of the drawbacks in the preceding studies, this paper plunges into research on a specific PHEB with the objective of improving overall vehicle fuel economy and the efficiency of individual components. The proposed approach involves a hybrid EMS based on intelligent algorithms and CDCS control rules, as well as a layered optimization method for powertrain parameters. It turns out to be viable to provide valuable insights for related studies in the field.

This article is arranged in the following format. The second section of the article describes the powertrain system model in detail. The MRB strategy for PHEB is presented as a proposed strategy in Section 3. In Section 4, the GOP method of powertrain parameter optimization is constructed. Section 5 outlines the results and discussion. In order to assess the efficiency of the energy management strategy and powertrain parameters method, Section 6 of the document is included.

2. Construction of an EMS Model and Parameter Matching for PHEB

Figure 1 [24] depicts the power-split PHEB structure researched in this paper. This system configuration involves the engine connected to the ring of the front planetary gear (PG1) and the carrier of the rear planetary gear (PG2). This design allows for the decoupling of the engine speed from the vehicle speed, accommodating significant variations in driving cycles.

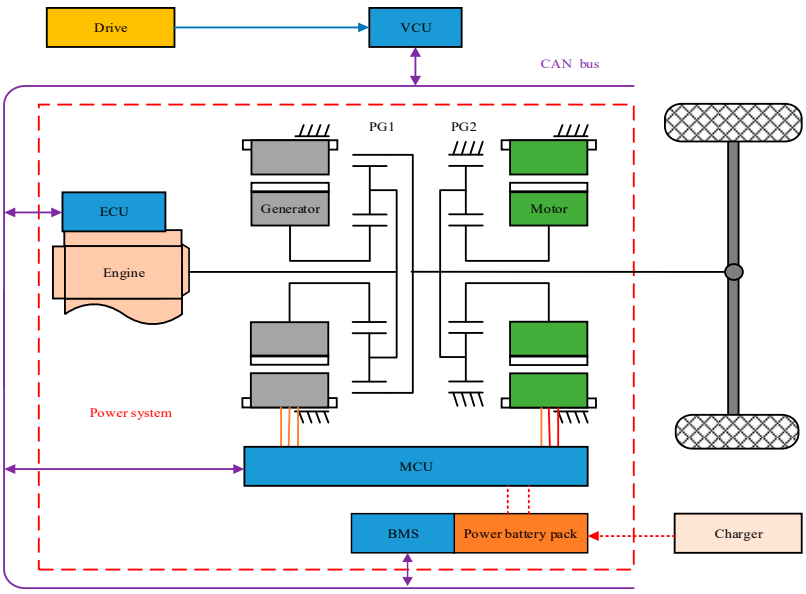

Figure 1. Configuration of the power-split hybrid powertrain structure.

2.1. Construction of a Full-Vehicle Model for PHEB

2.1.1. Longitudinal Dynamics Model of Vehicles

Based on the longitudinal kinematic equations of the vehicle, the expression for the power required to satisfy the driving is given by the following equation:

$$P_{dri}(t) = \frac{u(t)}{3600 \cdot \eta_m}\left(Mgf\cos\theta + \frac{AC_D u(t)^2}{21.15} + M\delta\cos\theta\frac{du}{dt} + Mg\sin\theta\right) \quad (1)$$

where P_{dri} denotes the driving power (kW); u denotes the vehicle speed (km/h); η_m denotes the mechanical efficiency of the powertrain components; M denotes the full-vehicle mass (kg); g denotes the gravitational acceleration (m/s^2); f denotes the rolling resistance coefficient; A denotes the windward area of the vehicle (m^2); C_D denotes the drag coefficient; δ denotes the coefficient of rotational inertia; and θ denotes the angle of the ramp (°).

Table 1 details the primary parameters for PHEB.

Table 1. Primary parameters for PHEB.

Parameter	Value	Unit
Full-vehicle mass	13,050	kg
Loaded mass	18,000	kg
Exterior dimension	12 × 2.55 × 3.2	m^3
Windward area	6.00	m^2
Drag coefficient	0.55	/
Rolling resistance coefficient	0.015~0.02	/
Wheelbase	6.05	m
Wheel rolling radius	0.512	m

2.1.2. Engine and Motor Models

For the engine and motor, the energy efficiencies based on steady-state experimental data can be represented as a function of speed and torque. Figures 2 and 3 [24] display the energy consumption maps for the engine and motor, respectively.

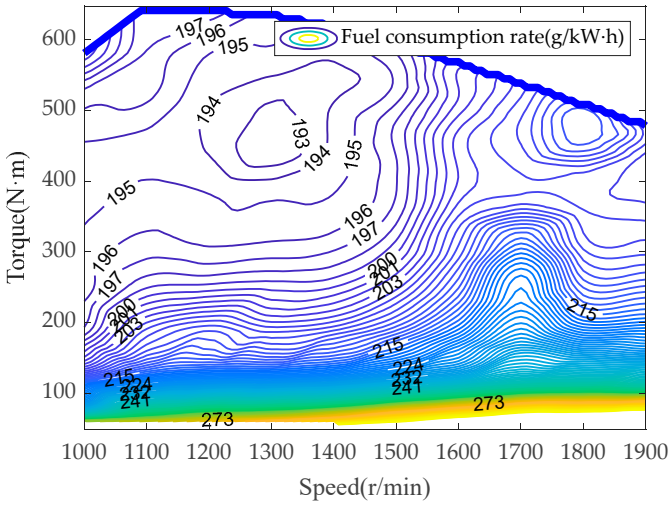

Figure 2. Universal characteristics map of the engine, adapted with permission from Ref [24]. Copyright 2023 Elsevier.

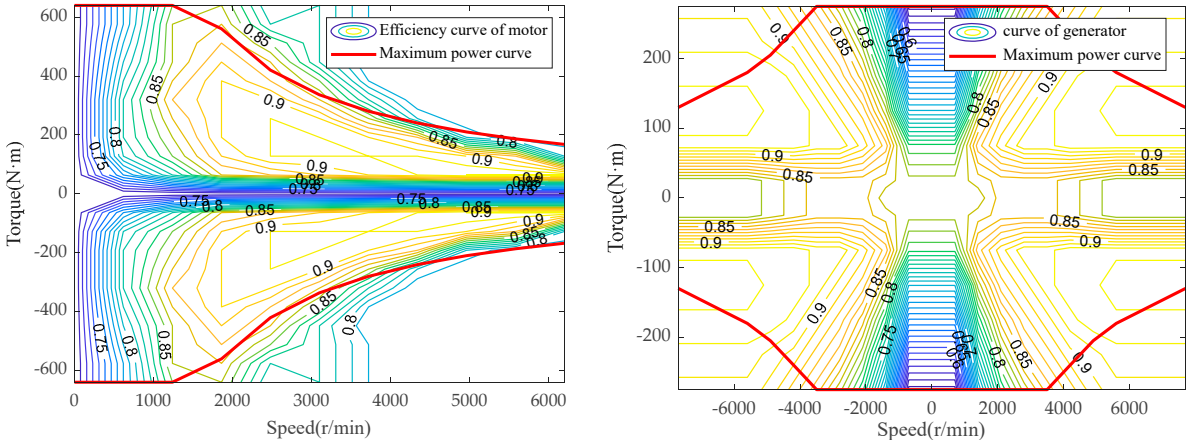

(**a**) (**b**)

Figure 3. Maps of the motor. (**a**) Drive motor; (**b**) generator, adapted with permission from Ref [24]. Copyright 2023 Elsevier.

2.1.3. Double-Planetary-Gear Coupling Mechanism Model

Depending on the connection relationship between each power source of the double-planetary-gear power-split PHEB and the double-planetary-gear mechanism, it is possible to derive the relationship between the torque and speed of the system, as illustrated in the following expression:

$$\begin{cases} T_{out} = T_{eng}\frac{\alpha_1}{1+\alpha_1} + T_{motor}(1+\alpha_2) \\ \omega_{out} = \frac{\omega_{motor}}{1+\alpha_2} = \frac{\omega_{eng}(1+\alpha_1)-\omega_{gen}}{\alpha_1} \\ \alpha_1 = (R_{s1}+R_{c1})/R_{c1} \\ \alpha_2 = (R_{s2}+R_{c2})/R_{c2} \end{cases} \quad (2)$$

where T_{out} and ω_{out} represent the torque and speed output from the double-planetary-gear coupling mechanism to the powertrain, respectively; T_{eng} and ω_{eng} represent the torque and speed of the engine, respectively; T_{motor} and ω_{motor} represent the torque and speed output from the drive motor, respectively; ω_{gen} represent the generator speed; α_1, R_{s1}, and R_{c1} represent the characteristic parameter, the sun wheel, and the planetary wheel radius of PG1, respectively; and α_2, R_{s2}, and R_{c2} represent the characteristic parameter, the sun wheel, and the planetary wheel radius of PG2, respectively.

2.1.4. Power Battery Models

1. Rint model of power batteries

The lithium iron phosphate ($LiFePO_4$) type, utilized as the power battery, employs the Rint model, as depicted in Figure 4. This battery comprised 157 cells arranged in series, with each cell boasting a capacity of 50 ampere-hours (A·h) and a voltage of 3.2 V. Consequently, the total voltage of the battery pack amounts to 502.4 V.

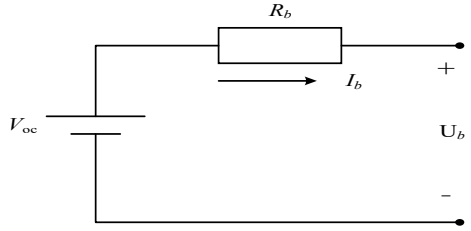

Figure 4. Rint model.

The SOC of the battery is calculated using the current integration method, represented by the following expression:

$$\mathrm{SOC}(t) = \mathrm{SOC}(t_0) - \eta_b^{\vartheta}(t)\int_{t_0}^{t_f} \frac{I_b(\tau)}{Q_{\mathrm{bat}}} d\tau \; I_b(t) > 0 \; \vartheta = -1; \; I_b(t) \leq 0 \; \vartheta = 1 \tag{3}$$

where SOC(t) indicates the SOC value of the battery at time t; SOC(t_0) indicates the SOC value of the battery at the initial time; t_0 and t_f indicate start and end moments at the current cycle; $\eta_b(t)$ indicates the battery efficiency at time t; $I_b(t)$ indicates the battery current at time t; Q_{bat} indicates the battery capacity; and ϑ indicates the index, with its value signifying charging and discharging, respectively.

2. Life model of power batteries

The cycling life of power batteries is a crucial factor influencing the operational costs of HEVs. Factors such as design, manufacturing processes, and operating environments all contribute to battery longevity. Prolonged battery life is advantageous for conserving societal resources and mitigating environmental pollution. This study zeroes solely on the battery's degradation process during use, discharge current, and ambient temperature, employing a semi-empirical battery aging model to construct a battery life degradation model. The maximum temperature of the battery is set at 35 °C. The model is expressed as follows:

$$Q_{loss} = B \exp\left(\frac{-E_a}{R(T + 273.15)}\right)(Ah)^z \tag{4}$$

where Q_{loss} represents the percentage of battery capacity loss; B is the pre-exponential factor with a value of 31,630; E_a denotes the activation energy; R is the universal gas constant with a value of 8.314 J/(mol·K); T represents the temperature in Kelvin; z is the power-exponent factor with a value of 0.57; and Ah signifies the total ampere-hour throughput.

To enhance the accuracy of the power battery's life model and its applicability in optimal control, parameter identification is performed using Equation (4) using experimental battery life data, yielding the refined battery capacity loss model expressed as follows:

$$Q_{loss} = (\alpha \mathrm{SOC} + \beta) \exp\left(\frac{-31700 + 163.3C}{R(T + 273.15)}\right)(Ah)^z \tag{5}$$

where α and β are constant terms, with their values specified in Equation (6), and C represents the battery discharge rate.

$$\begin{cases} \alpha = \begin{cases} 1287.6 & \mathrm{SOC} \leq 0.45; \\ 1385.5 & \mathrm{SOC} > 0.45, \end{cases} \\ \beta = \begin{cases} 6356.3 & \mathrm{SOC} \leq 0.45; \\ 4193.2 & \mathrm{SOC} > 0.45. \end{cases} \end{cases} \tag{6}$$

An aging factor, σ, is introduced to quantify the degree of battery aging under actual operating conditions compared to standard conditions. The expression for σ is given as follows:

$$\sigma(I, \theta, \mathrm{SOC}) = \frac{\Gamma_{real}}{\Gamma_{nom}} = \frac{\int_0^{EOL} |I_{real}(t)| dt}{\int_0^{EOL} |I_{nom}(t)| dt} \tag{7}$$

To quantify the capacity degradation during battery charging and discharging, the expression for ampere-hour throughput, Ah, is formulated as follows:

$$Ah = \int_{t_o}^{t_f} \sigma(I_b, T, \mathrm{SOC}) |I_b(t)| dt \tag{8}$$

2.2. Powertrain Parameter Matching in PHEB

This paper references standards such as the General Technical Requirements for Public City Bus [25] to match powertrain parameters based on CCBC, a typical urban bus driving cycle in China. The preliminary matching of power performance requirements and powertrain parameters for PHEB is outlined in Table 2.

Table 2. Power performance and powertrain parameters of PHEB.

Component	Parameter
Engine	Maximum power: 102 kW; Number of cylinders: 4; Cylinder diameter × cylinder stroke: 105 mm × 120 mm;
Drive motor	Rated power: 68 kW; Peak power: 106 kW; Peak torque: 620 N·m; Voltage platform: 600 V
Generator	Rated power: 60 kW; Peak power: 105 kW; Peak torque: 268 N·m; Voltage platform: 600 V
Double-planetary-gear coupling mechanism and powertrain	Characteristic parameters of PG1 and PG2: 2.6 and 2.6; Final drive ratio: 3.41
Power battery	Individual nominal capacity: 50 Ah; Rated voltage: 3.2 V; Continuous discharge capacity: 3 C; Instantaneous discharge: 10 C
Power battery pack	Voltage: 502.4 V; Number of batteries in series: 157; Number of batteries in parallel: 1

2.3. Experimental Conditions

This study takes a specific bus route in Xi'an City as a case study, with the tested route illustrated in Figure 5.

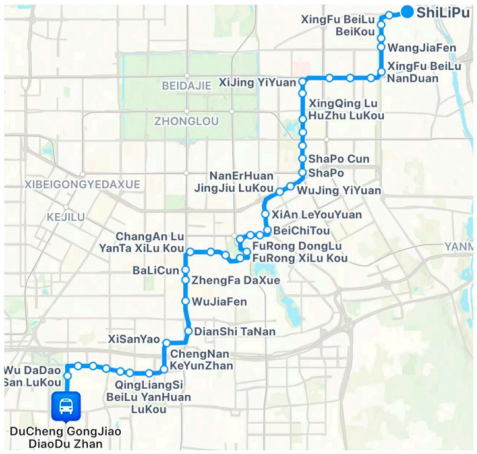

Figure 5. Tested bus route.

This route serves as a pivotal connection between the northeastern and southern outskirts of Xi'an, comprehensively covering congested urban segments, low-speed secondary roads, and medium-speed main arterials, thereby exhibiting a degree of representativeness. A comprehensive dataset of 3,608,753 valid speed records spanning 30 days was collected, from which 14 evaluative characteristic parameters, including peak speed, average speed, and speed standard deviation, were extracted. Subsequently, utilizing the Markov Chain Monte Carlo (MCMC) methodology, the operational condition of this route was synthesized, as depicted in Figure 6a, henceforth referred to as the synthetic driving cycle.

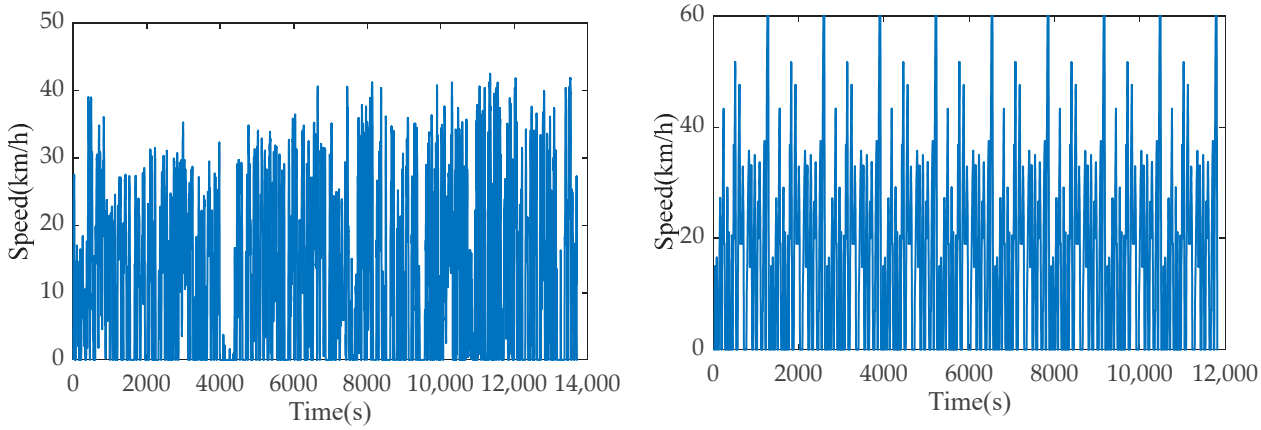

(**a**) (**b**)

Figure 6. Experimental conditions. (**a**) Synthetic driving cycle; (**b**) CCBC.

To validate the adaptability of our research approach, a composite scenario, integrating nine CCBC profiles, was constructed for comparative analysis, as presented in Figure 6b.

2.4. Model Verification

After the establishment of each component, the functional coordination and correctness of each module of the model are verified through simulation. The mathematical model of the whole vehicle is validated using synthetic working conditions.

As shown in Figure 7, under a synthetic driving cycle, the drive motor, generator, and engine work normally within the parameter range, and the torque outputs are also within the reasonable range; the power battery model also normally expresses the SOC changes of the charging and discharging state of the power battery.

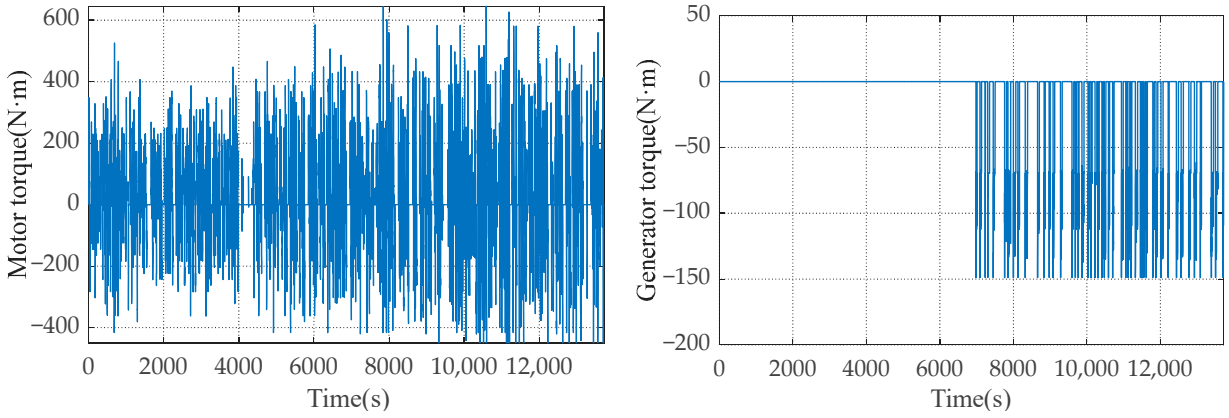

(**a**) (**b**)

Figure 7. *Cont.*

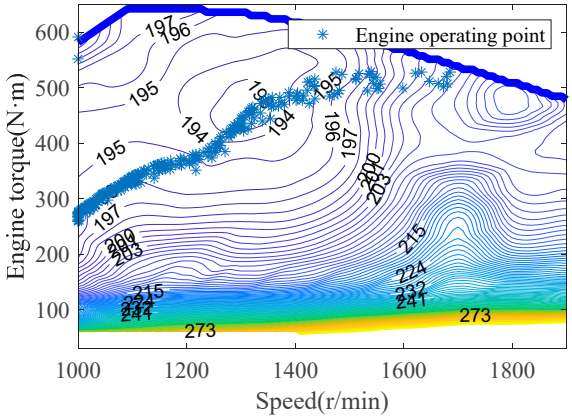

(**c**)

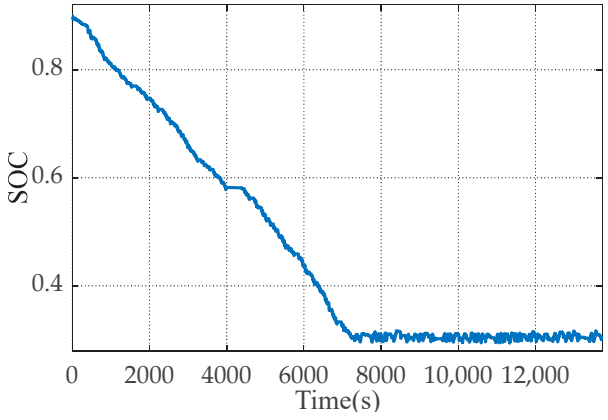

(**d**)

Figure 7. Simulation verification of various mathematical models. (**a**) Motor torque; (**b**) generator torque; (**c**) engine operating point; (**d**) SOC.

3. Study on Rule-Based EMS for PHEBs

3.1. Analysis of Operating Modes and System Efficiency of PHEBs

PHEB's operating modes determine the energy flow of various power sources in the hybrid powertrain and the operational status of its components. The vehicle state is defined as driving, idling, and braking. Based on engine operation and power battery charging/discharging states, PHEB's operating modes are categorized as Start (STA), Power Split (PS), Electric Driving (ED), Energy Recovery Charging (ERC), Mechanical Braking, and Shutdown Charging Hold (SCH) modes. Since this study revolves around energy allocation during PHEB driving, the charging mode from an external power grid and the complete shutdown mode are disregarded. Table 3 outlines the characteristics and efficiency of PHEB's operating modes.

Table 3. Characteristics and efficiency of PHEB's operating modes.

Vehicle State	Main Mode	Sub-State	Engine State	SOC	Efficiency Expression
Driving	Start (STA)		Startup	Discharge	$P_{sta} = \frac{\Delta\omega_{eng} \cdot I_{eng} \cdot \omega_{eng\_sta}}{573000 \cdot \eta_{gen}}$
	Power Split (PS)	Charge Depletion (CD)	Startup	Discharge	$\eta_{PS\text{-}CD}(t) = \frac{P_{motor}(t)+P_{eng\_dir}(t)}{P_{eng}(t)/\eta_{eng}(t)+P_b(t)}$
		Charge Sustaining (CS)	Startup	—	$\eta_{PS\_CS}(t) = \eta_{eng}(t)\frac{P_{motor}(t)+P_{eng\_dir}(t)}{P_{eng}(t)}$
		Charge Replenishment (CR)	Startup	Charge	$\eta_{PS\_CR}(t) = \eta_{eng}(t) \times \frac{P_{motor}(t)+P_{eng\_dir}(t)+P_b(t)}{P_{eng}(t)}$
	Electric Driving (ED)	Charge Depletion (CD)	Shutdown	Discharge	$\eta_{hm}(t) = \frac{P_{motor}(t)+P_{gen}(t)}{P_b(t)}$
Braking	Energy Recovery Charging (ERC)		Startup or Shutdown	Charge	$\eta_{rec}(t) = \frac{P_b(t)}{P_{motor}(t)}$
	Mechanical Braking		Startup or Shutdown	—	
Idling	Shutdown Charging Hold (SCH)		Startup	Charge	$\eta_{sch} = \frac{P_b(t)\cdot\eta_{eng}(t)}{P_{eng}(t)}$

where P_{sta} denotes the startup power; I_{eng} denotes the rotational inertia of the engine; ω_{eng_sta} denotes the startup speed of the engine; $P_{motor}(t)$, $P_{eng\_dir}(t)$, $P_{eng}(t)$, $P_{gen}(t)$, and $P_b(t)$ denote the drive motor power, the driving power output via the engine, the engine power, the generator power, and the battery power at time t, respectively; η_{gen} denotes the generator efficiency; $\eta_{PS\_CD}(t)$, $\eta_{PS\_CS}(t)$, $\eta_{PS\_CR}(t)$, $\eta_{hm}(t)$, $\eta_{rec}(t)$, and $\eta_{sch}(t)$ denote the system efficiencies under PS-CD, PS-CS, PS-CR, ED, ERC, and SCH modes at time t, respectively.

3.2. Multi-Layer Rule-Based Energy Management Strategy

This paper designs a multi-layer rule-based energy management strategy (MRB-EMS) capitalizing on the battery's SOC and its varying range. The fundamental control concept is to minimize the engine's fuel consumption under the current power conditions.

3.2.1. Design Concepts for the MRB Strategy

For a PHEB operating on a fixed route, ensuring sufficient SOC throughout its operation is crucial to meet the strategy's demands for energy. Therefore, in the design phase, after completing the final transport task, the power battery's charge is depleted to the lowest SOC. The expected target state of charge SOC_{tar} for the power battery is expressed as a function related to driving mileage, as shown in Equation (9).

$$SOC_{tar} = SOC(t_0) - \frac{SOC_{allow}}{S_{cyc\_d}} \cdot \int_{t_0}^{t_f} v(\tau) d\tau \quad (9)$$

where SOC_{allow} indicates the permissible discharge interval of the power battery and $S_{cyc\text{-}d}$ indicates the operating route distance.

The principle underlying the MRB strategy revolves around confining the current SOC as closely as possible to a predefined SOC_{tar} trajectory. This control strategy maintains the SOC within a corridor defined by an upper limit (SOC_{max}) and a lower limit (SOC_{min}) centered around the SOC_{tar}. Within this corridor, the CDCS strategy is employed. Specifically, when the SOC reaches the lower limit (SOC_{min}), the system transitions to a CS phase, where the vehicle is powered by the engine, enabling the SOC to disengage from the lower limit and ascend towards SOC_{max}. Conversely, upon reaching SOC_{max}, the system enters the CD phase, during which the SOC descends from the upper limit until it again reaches SOC_{min}, thereby maintaining a cyclical operation.

In summary, the MRB-EMS employs hard-switching rules at the outer layer that rely on the current battery SOC range to dictate operational modes. The inner layer, on the other hand, utilizes the CDCS strategy, which autonomously selects modes with SOC_{tar} as the control target.

As depicted in Figure 8, the CDCS strategy (represented by the red curve) prioritizes electric drive, resulting in a rapid decline in the SOC of the power battery. Upon reaching the lower SOC limit, the system transitions to the CS mode. In contrast, the MRB strategy (blue curve) features a function of the driving distance (SOC_{tar}), ensuring that the SOC reaches its lower limit upon completion of the operational task. The MRB strategy effectively constrains the battery's SOC around the SOC_{tar} trajectory.

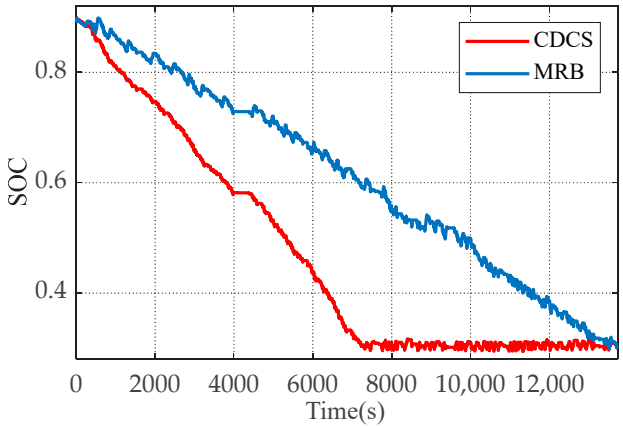

Figure 8. SOC trajectories of two strategies.

As evident in Figure 9a, from a fuel consumption perspective, the CDCS strategy, which prioritizes electric drive, fails to optimally blend fuel and electric power once the battery SOC reaches its lower limit, resulting in higher fuel consumption compared to the

MRB strategy. Conversely, Figure 9b illustrates that in terms of battery life, the preferential use of an electric drive in the CDCS strategy leads to a greater loss of battery life than in the MRB strategy. When entering the CD phase, the frequent charging and discharging cycles increase the cumulative ampere-hour throughput of the battery, thereby exacerbating the loss of the battery.

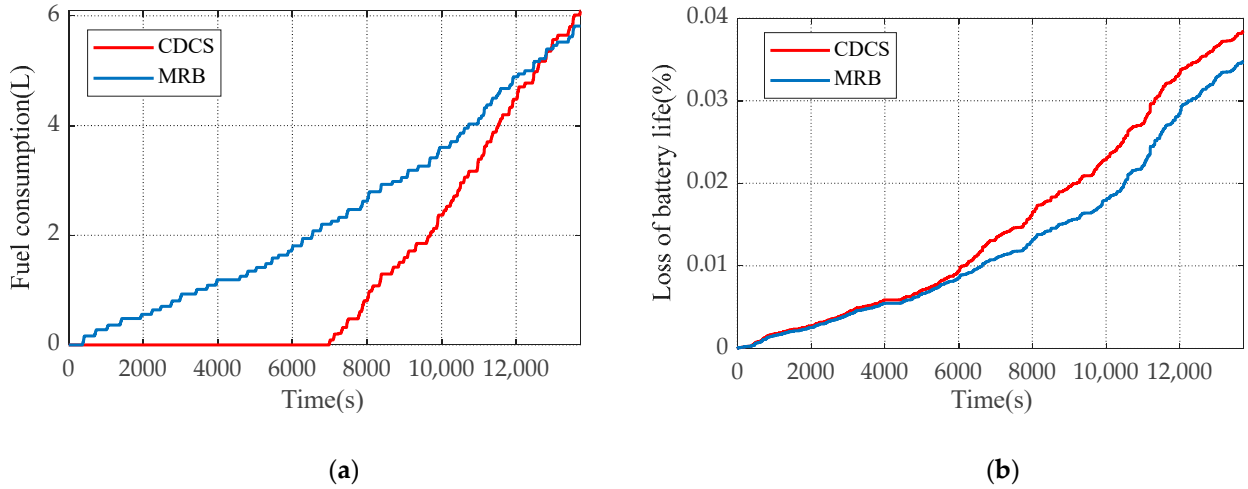

Figure 9. Performance analysis of the MRB algorithm. (**a**) Fuel consumption; (**b**) loss of battery life.

The MRB strategy significantly outperforms the CDCS strategy in terms of battery life preservation; however, further optimization is necessary to enhance its fuel economy.

3.2.2. Enhanced MRB Strategy

The inherent local CDCS strategy within the MRB framework at the inner layer suffers from limited adaptability due to its reliance solely on predefined rules. This section proposes an enhancement to the MRB strategy by incorporating an inner layer of adaptive switching rules designed through a fusion of intelligent algorithms and empirical knowledge. The algorithm computes the optimal driving strategy based on the required power (torque) and current vehicle speed, autonomously selecting either ED or PS mode. The core enhancements encompass the determination of driving mode selection and switching timings, specifically the transitions from ED to PS (ED-PS) and vice versa (PS-ED). This refined approach is subsequently designated as MRB-II, with the designed switching rules visualized in Figure 10.

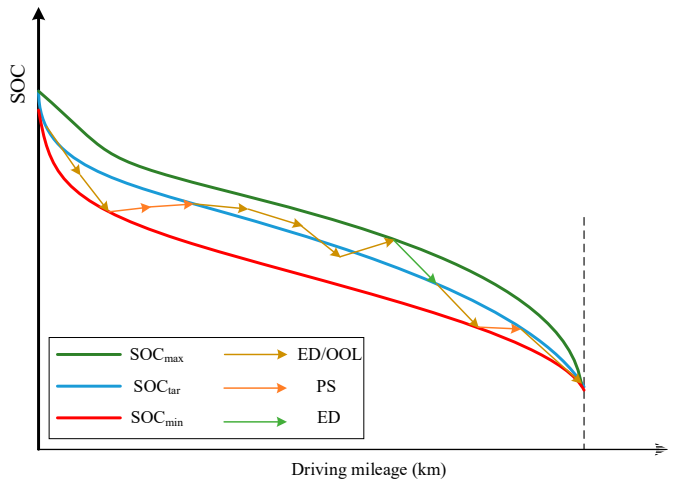

Figure 10. Operating principle of MRB strategy.

1. Formulation of the ED/OOL control rule

The Electric Driving/Optimal Operating Line (ED/OOL) strategy operates under the principle of utilizing a globally optimal Dynamic Programming (DP) algorithm to identify the most efficient operating mode for varying drive power requirements across all vehicle speeds. This process operates in reverse, tracing back to determine the optimal mode switching points.

According to the optimal control theory of DP, the cost function is expressed as follows:

$$\begin{cases} J_k^*(x(l)) = \min\{L_k(x(l), u(n)) + J_{k+1}^*(x(l), u(n)) \\ L_k(x(l), u(n)) = m_{fuel}(P_{eng}(n)) \end{cases} \tag{10}$$

where $J_k^*(x(l))$ denotes the minimum fuel consumption for the l-th state variable of the k-th discrete stage; $L_k(x(l), u(n))$ denotes the fuel consumption for the l-th state variable under the conditions of the k-th discrete stage and the n-th control variable; $J_{k+1}^*(x(l), u(n))$ denotes the minimum fuel consumption of the sub-stage for the l-th state variable and the n-th control variable in the $(k + 1)$-th discrete stage; m_{fuel} denotes the fuel consumption rate of the engine; and $P_{eng}(n)$ denotes the output power of the engine for the n-th control variable.

The expressions for the constraints that each component of the powertrain needs to satisfy are given below:

$$\begin{cases} T_{eng\_min} \le T_{eng} \le T_{eng\_max} \\ \omega_{eng\_min} \le \omega_{eng} \le \omega_{eng\_max} \\ T_{motor\_min} \le T_{motor} \le T_{motor\_max} \\ \omega_{motor\_min} \le \omega_{motor} \le \omega_{motor\_max} \\ T_{gen\_min} \le T_{gen} \le T_{gen\_max} \\ \omega_{gen\_min} \le \omega_{gen} \le \omega_{gen\_max} \\ \mathrm{SOC}_{min} \le \mathrm{SOC} \le \mathrm{SOC}_{max} \end{cases} \tag{11}$$

where subscripts _min and _max denote the lower and upper limits of the respective variables.

The solution process of the DP algorithm is illustrated in Figure 11.

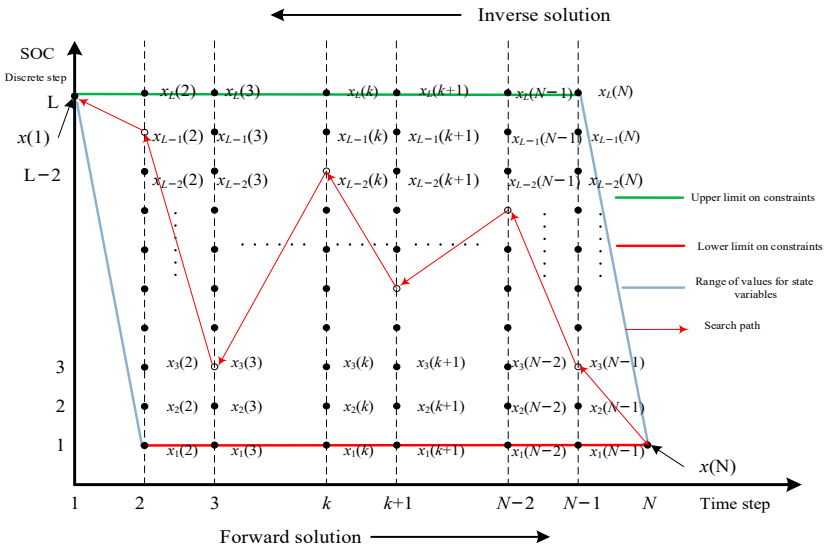

Figure 11. Solution process of the DP algorithm.

As shown in Figure 12, the PHEB's PS and ED modes are solved using the DP method; the curves represent the mode-switching boundaries. When the vehicle speed is constant, if the demand power transitions from below the red curve to above it, the PHEB mode switches to the PS mode; if the demand power transitions from above the blue curve to below it, the PHEB mode switches to the ED mode.

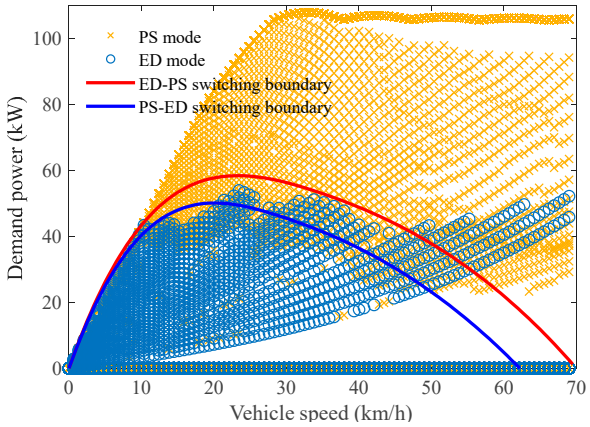

Figure 12. Operating points and mode-switching boundaries related to demand driving power and vehicle speed.

The switching rules of the MRB strategy at the outer layer are contingent upon the battery SOC. In contrast, the adaptive switching rules at the inner layer are determined by vehicle speed and demand power. The expressions are as follows:

$$\begin{cases} [SOC(t) \le SOC_{min}(t) | P_{dri}(t) > f_{E-P}(v(t))] \& \omega_{eng}(t) < 1000 & Model = 1 \\ [SOC(t) \ge SOC_{max}(t) | P_{dri}(t) \le f_{P-E}(v(t))] \& \omega_{eng}(t) \ge 1000 & Model = 2 \\ SOC(t) \le SOC_{min}(t) \& \omega_{eng}(t) \ge 1000 & Model = 3 \\ [SOC_{min}(t) \le SOC(t) \le SOC_{max}(t) \& P_{dri}(t) \ge f_{E-P}(v(t))] \& \omega_{eng}(t) \ge 1000 & Model = 4 \\ [SOC_{min}(t) \le SOC(t) \le SOC_{max}(t) \& P_{dri}(t) \le f_{P-E}(v(t))] \& \omega_{eng}(t) < 1000 | SOC(t) \ge SOC_{max}(t) & Model = 5 \\ [SOC(t) < SOC_{tar}(t) \& v(t) = 0] \& Model_{front} = 3 & Model = 6 \end{cases} \quad (12)$$

where Model = 1 represents the STA mode; Model = 2 represents the shutdown mode of the engine; Model = 3 represents the low battery forced hybrid mode; Model = 4 represents the OOL hybrid mode; Model = 5 represents the ED mode; Model = 6 represents the SCH mode; $f_{E\text{-}P}(v(t))$ represents the upper limit for ED mode switching to PS mode; $\omega_{eng}(t)$ represents the engine speed at time t; $f_{P\text{-}E}(v(t))$ represents the lower limit for PS mode switching to ED mode; $SOC_{min}(t)$ and $SOC_{max}(t)$, respectively, represent the lower and upper limits of SOC at time t; Modelfront denotes the system mode in the previous state; $SOC_{tar}(t)$ represents the target SOC value at time t; and P_{dri} represents the driving power at time t.

2. Mode-switching logic of the MRB strategy

Figure 13 presents the mode-switching logic of the MRB strategy formulated by the Stateflow platform.

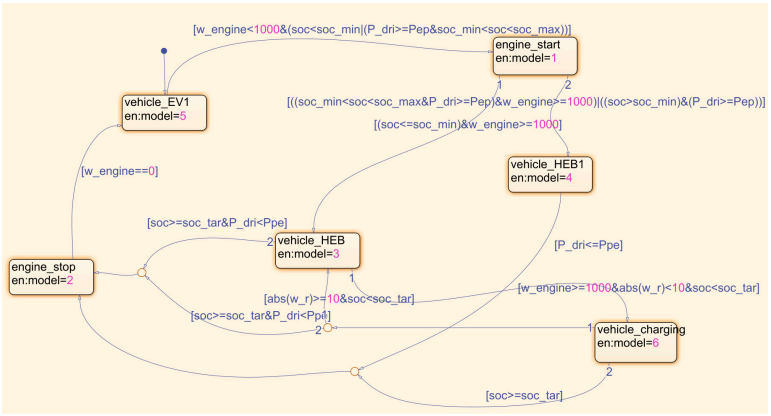

Figure 13. Logic of MRB strategy under Stateflow environment.

3.3. Performance Test of MRB-EMS

To validate the performance and adaptability of the algorithms, a comparative analysis of three strategies was conducted under two distinct operating conditions.

As elucidated in Figure 14a,b, the MRB-II strategy exhibits a more linear variation in SOC, resulting in a smoother discharge of the power battery under both operating conditions. The fuel consumption, shown in Figure 14c,d, is further reduced by the MRB-II strategy due to its adaptive selection of optimal driving modes within the powertrain system, outperforming the conventional MRB strategy. As illustrated in Figure 14e,f, the smoother SOC profiles mitigate high-power, repetitive charge–discharge cycles of the power battery, leading to a decrease in accumulated Ampere-hours throughput and suppression of aging factors, thereby significantly reducing the loss of battery life.

Ultimately, as evidenced in Table 4, under the CCBC conditions, MRB-II demonstrates a 12.02% reduction in fuel consumption and a 33.33% decrease in loss of battery life compared to the CDCS strategy. Likewise, under synthetic driving cycles, fuel consumption drops by 10.35%, and loss of battery life is reduced by 31.64%. These results underscore the substantial improvement in fuel economy and the remarkable effectiveness of MRB-II in preserving battery health.

Table 4. Comparative Analysis of MRB-II Performance.

EMS	Fuel Consumption (L)		Loss of Battery Life (%)	
	CCBC	Synthetic Driving Cycle	CCBC	Synthetic Driving Cycle
CDCS	6.0907	6.0308	0.0384	0.0275
MRB	5.8149	5.8671	0.0347	0.0211
MRB-II	5.3586	5.4064	0.0256	0.0188
MRB-II vs. CDCS	−12.02%	−10.35%	−33.33%	−31.64%

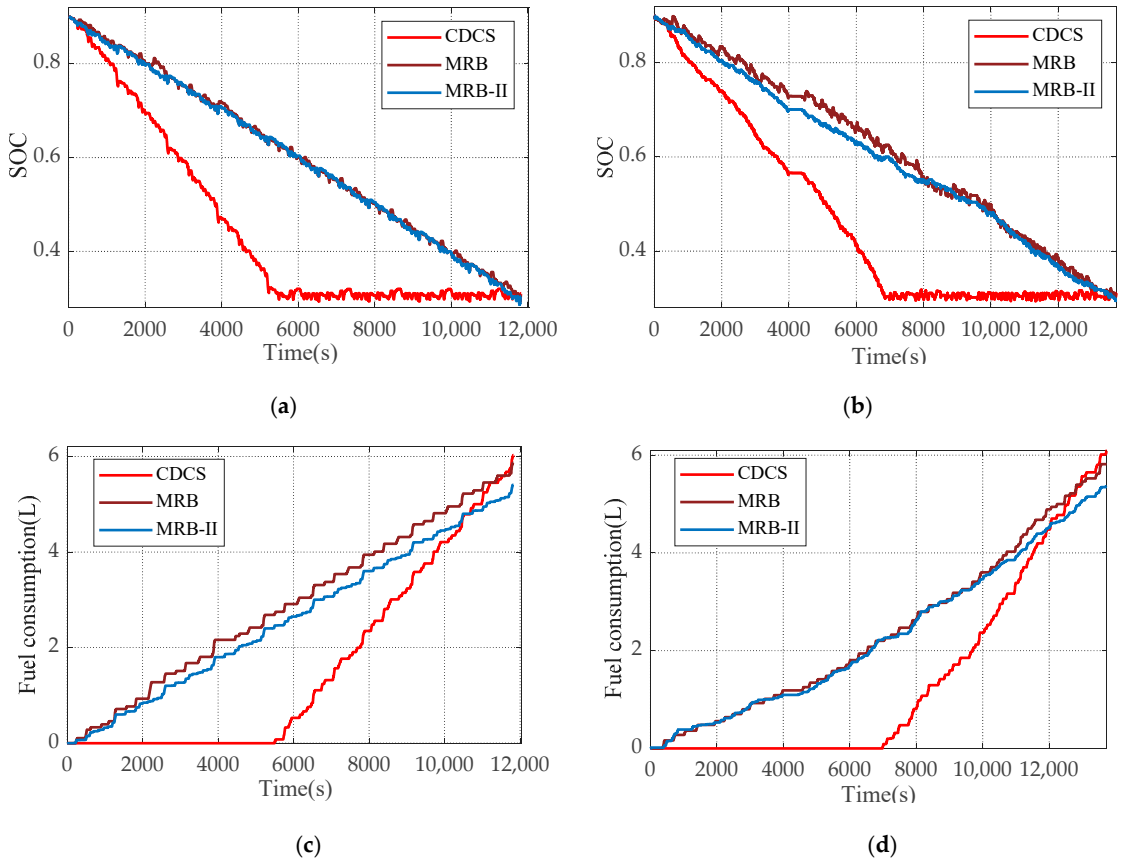

Figure 14. *Cont.*

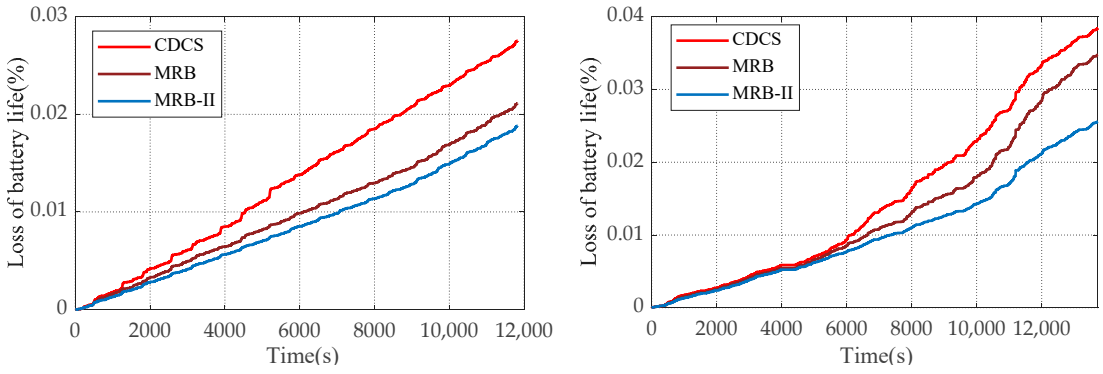

(**e**) (**f**)

Figure 14. Comparison of the performance of MRB-II with other strategies. (**a**) SOC under CCBC; (**b**) SOC under synthetic driving cycle; (**c**) fuel consumption under CCBC; (**d**) fuel consumption under synthetic driving cycle; (**e**) loss of battery life under CCBC; (**f**) loss of battery life under synthetic driving cycle.

In the power-split PHEB hybrid powertrain, energy management strategies and design parameters of the powertrain are interdependent, collectively influencing the vehicle's performance in terms of power, economy, and emissions. Hence, to achieve design goals like fuel efficiency and power performance, simultaneous optimization of both energy management strategies and powertrain parameters is necessary.

4. Optimization of Powertrain Parameters Based on the GOP Method

The vehicle's energy consumption during operation indirectly reflects drive efficiency, suggesting that higher overall drive efficiency correlates with better energy conversion in the drive system. Optimizing powertrain parameters can enhance the powertrain efficiency to some extent. This section focuses on achieving optimal working efficiency of the powertrain. With the characteristic parameters of the front and rear planetary gear sets along with the final drive ratio as optimization parameters, it proposes a multi-layer powertrain optimization method using the GOP.

4.1. Selection of Powertrain Parameters Based on the Genetic Algorithm

The optimization process involves using a GA to search for the optimal parameters of powertrain components, aiming to maximize the overall vehicle drive efficiency. The objective function is formulated based on maximizing efficiency, and the expression is as follows:

$$\begin{cases} J_{sys} = \max(\dfrac{A_1}{B_1}) \\ A_1 = \sum\limits_{t_0}^{t_f}[(P_{motor}(t) + P_{eng\_dir}(t))\cdot(Stu(t) = 1|3) + (P_{motor}(t) + P_{eng\_dir}(t) + P_b(t))\cdot(Stu(t) = 2) \\ \quad + |P_{motor}(t) + P_{gen}(t)|\cdot(Stu(t) = 4) + (P_b(t)\cdot Stu(t) = 5|6)] \\ B_1 = \sum\limits_{t_0}^{t_f}[(\dfrac{P_{eng}(t)}{\eta_{eng}(t)} + P_b(t))\cdot(Stu(t) = 1) + \dfrac{P_{eng}(t)\cdot(Stu(t) = 2|3|6)}{\eta_{eng}(t)} \\ \quad + P_b(t)\cdot(Stu(t) = 4) + P_{motor}\cdot(Stu(t) = 5) + P_{sta}\cdot(Stu(t) = 7] \end{cases} \quad (13)$$

where J_{sys} represents the objective function; A_1 and B_1 represent intermediate variables, respectively; $Stu(t)$ represents the correspondence between the values of the vehicle powertrain's operating sub-state at time t and the system state. The expression is as follows:

$$\begin{cases} \mathrm{Stu}(t) = 1 & \text{PS-CD} \\ \mathrm{Stu}(t) = 2 & \text{PS-CS} \\ \mathrm{Stu}(t) = 3 & \text{PS-CR} \\ \mathrm{Stu}(t) = 4 & \text{ED} \\ \mathrm{Stu}(t) = 5 & \text{REC} \\ \mathrm{Stu}(t) = 6 & \text{SCH} \\ \mathrm{Stu}(t) = 7 & \text{STA} \end{cases} \tag{14}$$

When the system is in PS mode, the states correspond to the current state of the power battery current (positive, negative, or zero) as follows: Stu(t) = 1 for positive, Stu(t) = 2 for negative, and Stu(t) = 3 for zero current. Under the condition that the engine output power is zero and the power battery current is positive, Stu(t) = 4. For negative power in the drive motor, Stu(t) = 5. When the engine's output power is positive and the vehicle speed is zero, Stu(t) = 6. When the engine speed increases from zero to idle, Stu(t) = 7.

The constraints for the objective function considering the limitations of powertrain speed and vehicle speed, determined during the comprehensive model construction, are as shown in Equation (15).

$$\begin{cases} \alpha_{1\_min} \le \alpha_1 \le \alpha_{1\_max} \\ \alpha_{2\_min} \le \alpha_2 \le \alpha_{2\_max} \\ \mathrm{i}_{0\_min} \le \mathrm{i}_0 \le \mathrm{i}_{0\_max} \\ \frac{60 \times \mathrm{v}_{max} \times \mathrm{i}_0 \times (1+\alpha_2)}{2 \times \pi \times \mathrm{r}_{tire}} \le \omega_{motor\_max} \\ -\frac{60 \times \mathrm{v}_{max} \times \mathrm{i}_0 \times \alpha_1}{2 \times \pi \times \mathrm{r}_{tire}} \le \omega_{gen\_min} \\ \omega_{eng\_max} \times (1+\alpha_1) - \frac{60 \times \mathrm{v}_{max} \times \mathrm{i}_0 \times \alpha_1}{2 \times \pi \times \mathrm{r}_{tire}} \le \omega_{gen\_max} \end{cases} \tag{15}$$

where subscripts_min and_max denote the lower and upper limits of the respective variables.

Regarding this optimization problem, GA determines the population, evaluation function, selection operator, individual encoding, mutation operation, etc. The obtained optimal individual is then considered as the final powertrain parameters selected by the system. For a comprehensive optimization of the overall system efficiency, considerations extend to the efficiency of the ED mode and the SCH mode. This section designs a dual-motor hybrid drive strategy and an optimal strategy for efficiency in the SCH mode.

4.2. Optimal Adaptive Control of Motor Efficiency (OAME) Strategy

This section outlines the design of the OAME strategy. This strategy calculates and solves for the optimal efficiency point of the motor system (drive motor and generator) at different output coefficients under current conditions of vehicle speed and required driving power. It then adopts the optimal output coefficient as the current electric drive policy to ensure that all motors operate at their highest drive efficiency in ED mode. The OAME strategy overcomes the limitations of traditional methods and addresses the complexity and real-time optimization challenges associated with global optimization calculations.

The system efficiency and output torque expressions for the dual motors in the PHEB under the ED mode are given as follows:

$$\begin{cases} \eta_{sys} = \frac{\mathrm{P}_{motor} + \mathrm{P}_{gen}}{\mathrm{P}_{motor}/\eta_{motor}(\mathrm{T}_{motor}, \omega_{motor}) + \mathrm{P}_{gen}/\eta_{gen}(\mathrm{T}_{gen}, \omega_{gen})} \\ \mathrm{T}_{motor} = \frac{\mathrm{T}_{dri} \times \kappa}{1+\alpha_2} \\ \mathrm{T}_{gen} = \frac{\mathrm{T}_{dri} \times (1-\kappa)}{\alpha_1} \end{cases} \tag{16}$$

where η_{sys} denotes the efficiency of the motor system and κ denotes the output coefficient in ED mode in the range of [0, 1].

Here is a step-by-step breakdown of the specific optimization calculation process:

(1) Check the operating state of the PHEB. If the PHEB operates in any state other than ED mode (Stu $\neq$ 4), set the optimal output coefficient $\kappa* = 1$. Otherwise, proceed to step (2).
(2) Discretize the output coefficient κ. Discretize the dual-motor drive output coefficient κ with a step size of s_β. $\kappa_i \in [0: s_\beta: 1]$, where $i = 0, 1, 2, \ldots, 1/s_\beta$, and i represents the subscript of the i-th discrete output coefficient.
(3) Calculate the optimal output coefficient $\kappa*$ for the drive motor. Iterate through and store the system efficiency for each output coefficient κ_i. Save κ_i under the highest system efficiency, and $\kappa* = \kappa_i$.
(4) Output $\kappa*$.
(5) Repeat steps (1) to (4) until the end of the driving cycle.

Simulation results of forcibly placing the vehicle into ED mode under CCBC are illustrated in Figures 15–18.

As observed in Figure 15a, under the OAME strategy, the generator shares part of the torque of the drive motor, causing the operating point of the drive motor to move closer to the high-efficiency (red dots) points. This advantage of the dual-motor drive is particularly evident when the speed is above 2300 r/min and the torque is greater than 200 N·m or when the speed is below 1000 r/min and the torque is greater than 220 N·m. Figure 15b displays the operating points of the generator driven by the OAME strategy. Particularly, when the vehicle's speed and torque demand are low, the vehicle is entirely driven by the generator output, giving full play to the high-efficiency characteristics of the generator in that range. When the drive motor features high speed and high torque demand or low speed and significant torque demand, the generator and drive motor work together to output the driving power.

As depicted in Figure 16, the red triangles represent OAME-HM, which denotes the system efficiency during motor system operation. It is observable that at any operating point, the OAME-HM efficiency is greater than or equal to the efficiency of the single-drive motor (black dots). When the system operates in a dual-motor hybrid drive mode, the system efficiency lies between the efficiency of the current drive motor and that of the generator, embodying the optimal state. In Figure 17, at the end of the cycle, considering solely energy consumption, the energy consumption of the vehicle in single-motor drive mode is 1.343 $\times$ 10^7 J, while under the OAME strategy, it is 1.228 $\times$ 10^7 J. The OAME strategy reduces energy consumption by 8.562%, demonstrating a significant improvement in energy efficiency.

Simulation results indicate that the OAME strategy effectively enhances the economy in ED mode compared to single-drive motors, resulting in reduced energy consumption in ED mode.

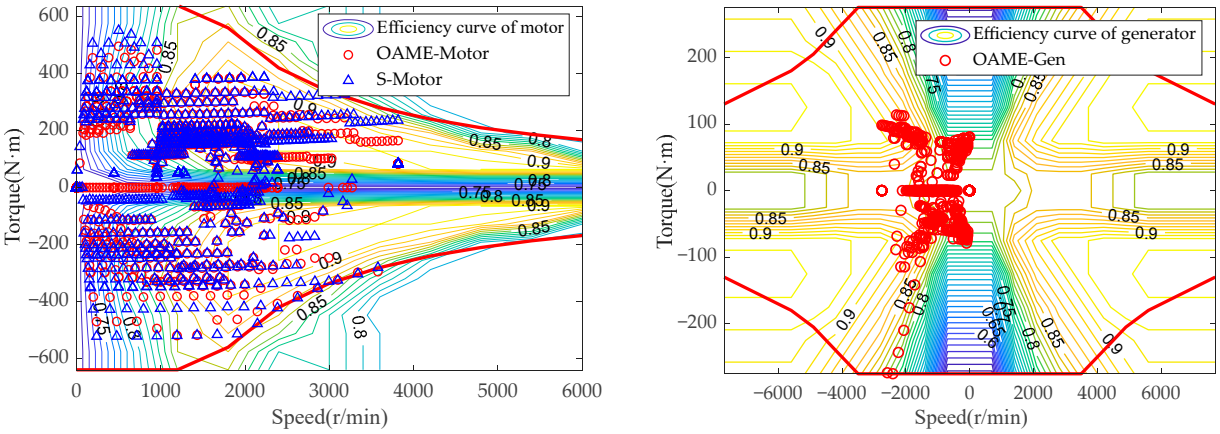

(**a**) (**b**)

Figure 15. Distribution of operating points of the motor system under the OAME strategy. (**a**) Distribution of operating points of drive motors; (**b**) distribution of operating points of generators.

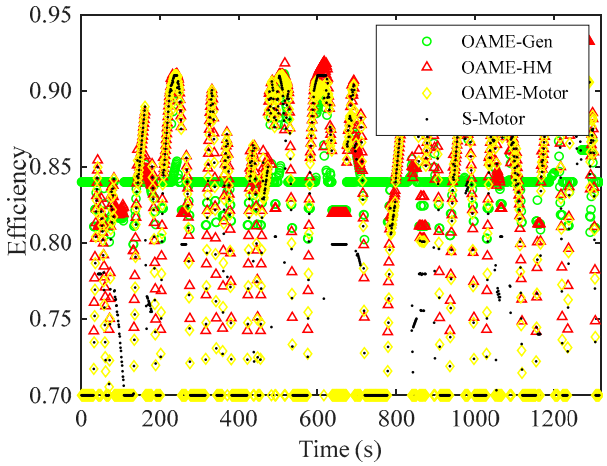

Figure 16. Comparison of the efficiency of motors.

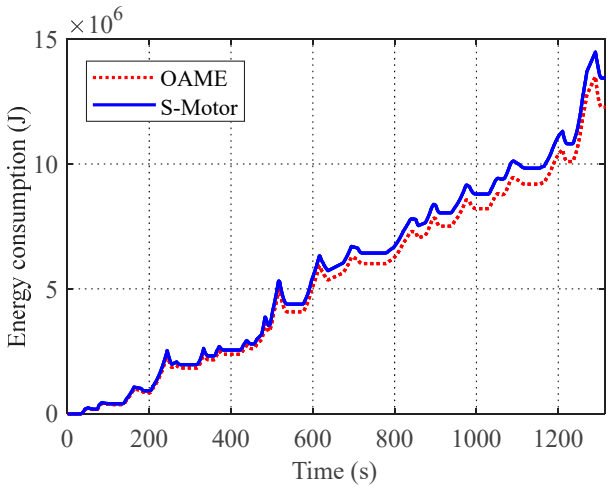

Figure 17. Energy consumption comparison.

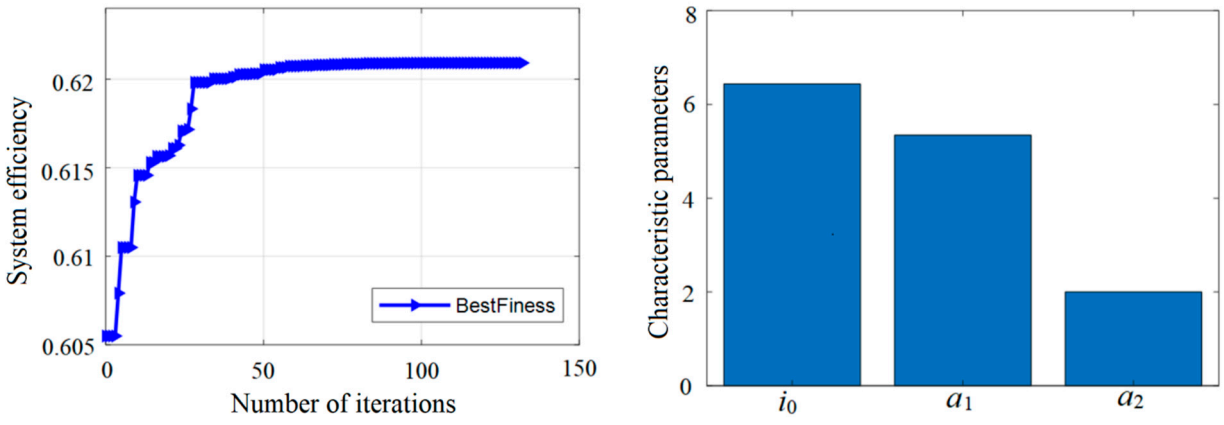

(**a**) (**b**)

Figure 18. *Cont.*

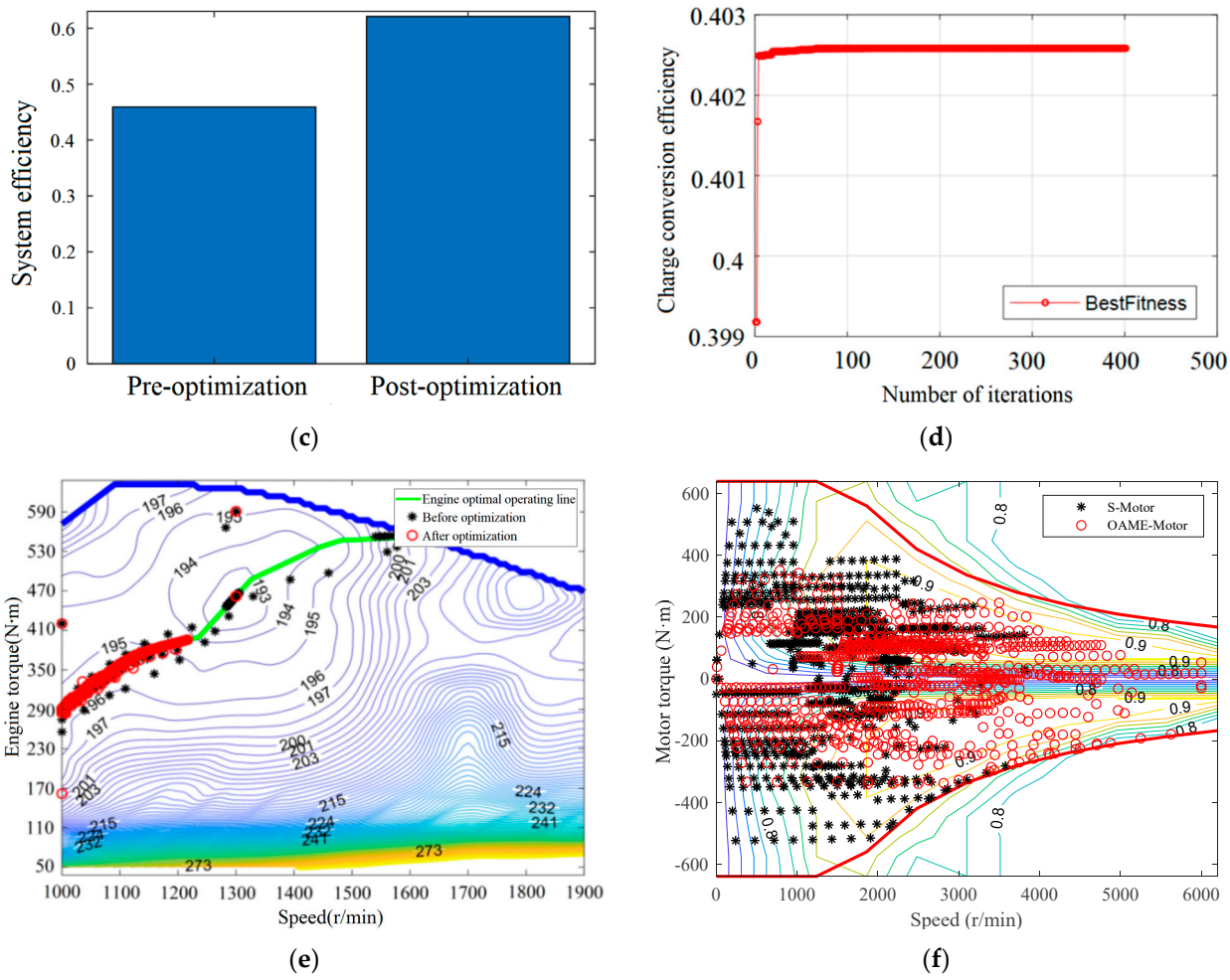

Figure 18. Analysis of optimization results using the GOP method. (**a**) GA iteration results; (**b**) post-optimization parameters; (**c**) comparison of pre and post-optimization system efficiencies; (**d**) PSO solution results; (**e**) comparison of engines' operating points; (**f**) comparison of drive motors' operating points.

4.3. Optimization of SCH Based on the Particle Swarm Optimization (PSO) Algorithm

The PSO algorithm stems from Reynolds' proposal based on the foraging behavior of bird flocks. When dealing with problems involving continuous variables, the PSO algorithm demonstrates characteristics such as low computational complexity and rapid convergence. The operational state of an engine can be viewed as a continuous variation in both speed and torque. Hence, this section employs the PSO algorithm to determine the optimal operating point for the engine in the SCH mode.

In the SCH mode, the engine's output power is entirely transmitted to drive the generator for power generation through the planetary carrier. The efficiency of both the engine and generator varies at different torque and speed states. As the optimal state remains constant, the calculation of its system efficiency can be regarded as a steady-state process, expressed as follows:

$$\eta_{rec} = \eta_{eng} \cdot \eta_{gen} \tag{17}$$

$$J_{rec} = -\eta_{eng} \cdot \eta_{gen} \tag{18}$$

The optimization process involves solving a single-objective dual-parameter problem. Therefore, the number of particles is 2, denoted as P_1 and P_2, with both in the range [0, 1]. The conditional expression is given below:

$$\begin{cases} \omega_{eng} = \omega_{eng\_min} + P_1 \cdot (\omega_{eng\_max} - \omega_{eng\_min}) \\ T_{eng} = T(\omega_{eng})_{min} + P_2 \cdot (T(\omega_{eng})_{max} - T(\omega_{eng})_{min}) \\ \omega_{gen} = \omega_{eng} \cdot (1 + \alpha_1) \\ T_{gen} = T_{eng} / (1 + \alpha_1) \\ \eta_{eng} = f(T_{eng}, \omega_{eng}) \\ \eta_{gen} = f(T_{gen}, \omega_{gen}) \end{cases} \quad (19)$$

where $T(\omega_{eng})_{min}$ signifies the minimum torque at the current engine speed and $T(\omega_{eng})_{max}$ signifies the maximum torque at the current engine speed.

The PSO algorithm tracks the historical optimal positions of individuals and the population. It continuously updates and iterates the particle's velocity and position information through two behaviors, exploration and exploitation, to achieve the evolution of the population. The main parameters of the PSO algorithm include the population size (M_{PSO}), search space dimension (D), maximum number of iterations (G), maximum velocity of the particle (v_{p_max}), weight coefficient (ω) representing the global and local search capabilities of the particle, and learning factors c_1 and c_2 (generally set as 2). The optimization process of the PSO algorithm involves initializing particles' speed and position variables, determining the individual historical optimal position and the population's historical optimal position, and determining the particle's speed and position for the next iteration to optimize the optimal operating point for the engine during the SCH mode.

To put it in a nutshell, the optimization algorithm for powertrain parameters in this section consists of three layers: the top layer is the objective layer, the middle layer is the control strategy algorithm layer, and the bottom layer is the model layer. The powertrain parameters optimized by the GA via the OAME strategy and PSO algorithm are utilized to calculate the optimal output coefficient $\kappa*$ of the dual motors and the engine's speed and torque during the SCH mode. These parameters are then passed to the MRB strategy. The model layer utilizes the control algorithm to transmit various component control signals to the vehicle model, iteratively generating the fitness function values required for the GA. Figure 18 represents the overall topology of the GOP method.

5. Results and Discussion

Figure 18 represents the optimization results of the PHEB's powertrain parameters using the GOP method.

As depicted in Figure 18a, after 137 iterations of the algorithm, the model acquired the optimal powertrain parameters shown in Figure 18b. The resulting parameters were α_1 = 5.346, α_2 = 2, and i_0 = 6.434.

In Figure 18c, with initial parameters of α_1 = 2.6, α_2 = 2.6, and i_0 = 3.41, the system efficiency was 0.4637. Post-optimization, the powertrain, as illustrated in Figure 18d, revealed the highest efficiency of 0.4026 for the SCH mode. At this point, the engine speed was 1318 r/min, with a torque of 429.2 N·m.

In Figure 18e, compared to the pre-optimization state where a substantial number of the engine's operating points were concentrated at a higher speed of 1600 r/min, resulting in fuel consumption of 202 g/(kW·h), after the GOP optimization, the engine's operating points shifted toward lower-speed regions. The fuel consumption in this region was approximately 195~196 g/(kW·h), indicating a notable enhancement in the engine's fuel conversion efficiency.

As demonstrated in Figure 18f, post-optimization, the overall load on the drive motor decreased, and the operating points shifted toward high-efficiency points. Particularly in the ERC mode, the efficiency of the motor under the OAME strategy significantly improved, reaching 0.621. This enhancement led to a 33.92% improvement in the overall vehicle system efficiency.

To validate the adaptability and effectiveness of the GOP optimization, a comparative analysis of the powertrain parameters before and after optimization was conducted under CCBC and synthetic driving cycles. Following optimization, the increase in the charac-

teristic parameters of the front planetary gear enhanced the direct torque transmission from the engine to the front gear ring via the planet carrier, improving the powertrain efficiency during PS phases. Additionally, it harnessed the inherent efficiency advantage of the generator at higher rotational speeds, resulting in enhanced power generation efficiency. Conversely, the decrease in the characteristic parameters of the rear planetary gear, coupled with an increase in the final drive ratio, reduced the load on the drive motor. This shift allowed the operating point to move towards the high-efficiency points, consequently enhancing the efficiency of the drive motor.

As witnessed in Figure 19, the optimized powertrain system facilitated the shift of engine operating points from high-load to medium-to-low-load regions, resulting in enhanced engine efficiency. The OAME strategy contributed to bolstering the electric drive efficiency of the individual motor, as evidenced in Table 5. Upon GOP optimization, the fuel consumption under CCBC conditions decreased from 5.35 L to 4.87 L, representing a 9.04% reduction in the cycle fuel consumption. Similarly, loss of battery life declined from 0.0188% to 0.0182%, a 3.19% improvement. Under synthetic driving cycles, fuel consumption dropped from 5.41 L to 4.43 L, translating into an 18.11% reduction, while battery life loss decreased from 0.0256% to 0.0237%, a 7.32% improvement. These simulation results conclusively demonstrate that GOP-optimized powertrain parameters enhance the overall efficiency of the powertrain system, as corroborated by their abilities to improve vehicle-level fuel economy and mitigate the loss of battery life, underscoring the practicality and efficacy of the optimization approach.

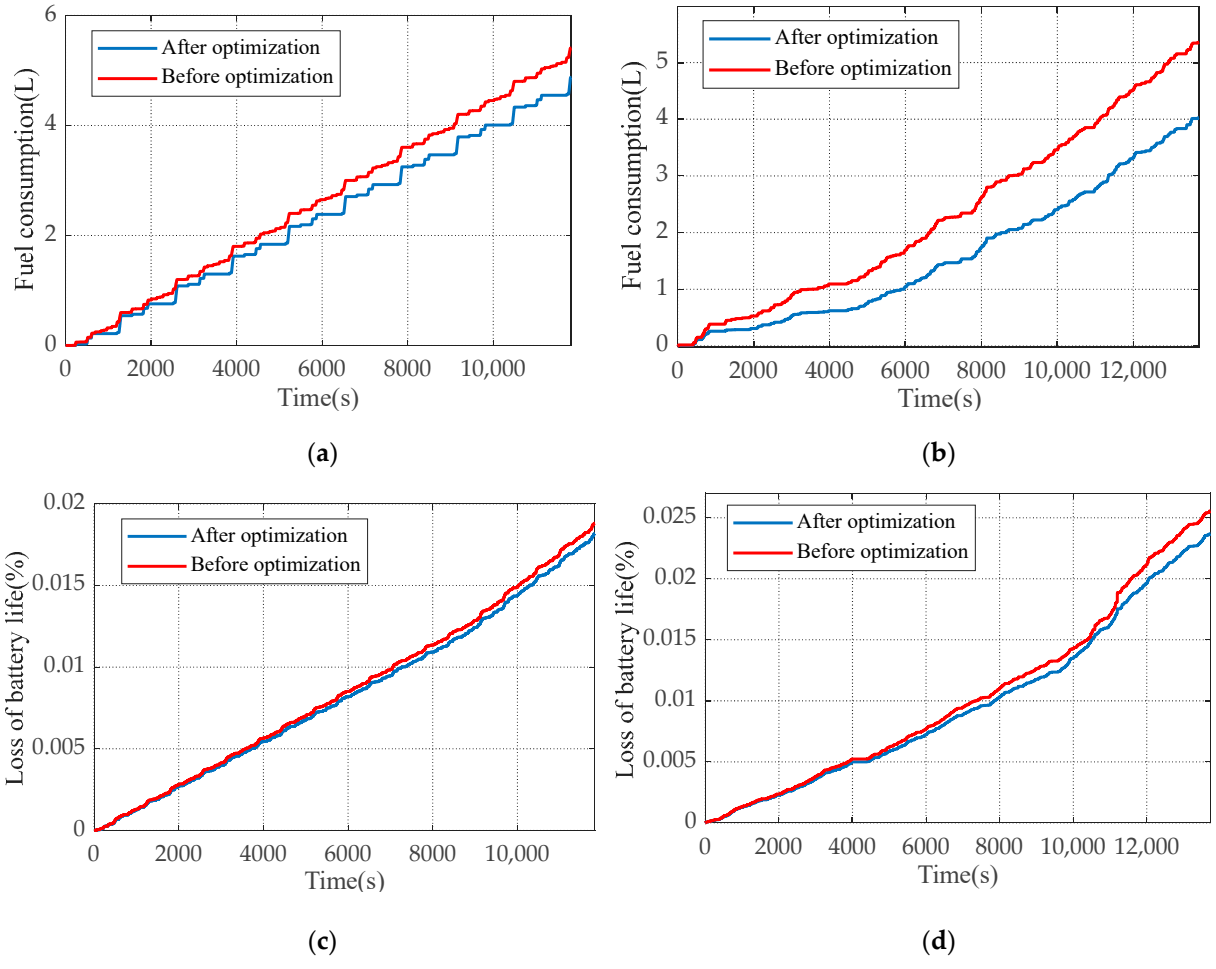

Figure 19. Comparison of fuel consumption and loss of battery life before and after GOP optimization. (**a**) Fuel consumption under CCBC; (**b**) fuel consumption under synthetic driving cycle; (**c**) loss of battery life under CCBC; (**d**) loss of battery life under synthetic driving cycle.

Table 5. Comparison of evaluation metrics.

State	Fuel Consumption (L)		Loss of Battery Life (%)	
	CCBC	Synthetic Driving Cycle	CCBC	Synthetic Driving Cycle
Before optimization	5.3586	5.4064	0.0188	0.0256
After optimization	4.8743	4.4275	0.0182	0.0237
Before vs. After	−9.04%	−18.11%	−3.19%	−7.42%

In this study, the positive points of the proposed methodology are as follows:

1. In this paper, an oil–electric control method based on the target SOC trajectory is designed for the line operation characteristics of PHEBs. This solves the problem that the conventional CDCS strategy fails to control the power source according to the preset SOC trajectory.
2. To further improve the efficiency of the ED mode, this paper designs an OAME strategy to achieve the highest efficiency of the electric drive system. By evaluating the efficiency of the motor system in the ED mode, this strategy automatically seeks the optimization in the current state, the single generator mode, the single drive motor mode, and the dual motor mode, thus attaining minimal electric energy consumption in the ED mode.
3. In this paper, to solve the problem of fuel consumption efficiency in parking power generation mode, the PSO algorithm is used to dynamically solve the optimal engine operating point under different driveline parameters, resulting in the most efficient fuel consumption in this mode.
4. Recognizing the direct correlation between the characteristic parameters of the power coupling mechanism and the overall mixing efficiency, the GA algorithm is leveraged to optimize drivetrain parameters with the objective of enhancing vehicle power system efficiency. This offline optimization process yields optimal characteristic parameters that elevate the powertrain system's efficiency.
5. The DP algorithm is harnessed to pinpoint the optimal efficiency of the powertrain system's operating point under arbitrary power and rotational speed conditions, thereby achieving minimal energy consumption.
6. The statistical method is used to design the PS-ED and ED-PS switching demarcation line, which can effectively avoid the problem of repeated switching of PS and ED in the power system at the efficiency critical point.

The limitations of this paper are as follows:

1. While the paper is based on the flat terrain of Xi'an City, if the operating line is in an area with significant altitude fluctuations, the SOC target trend based on the operating mileage cannot fully reflect the distribution of power in each stage.
2. For the inner logic layer of MRB-II, there is still room for improvement in the intelligence of mode switching for rule-based switching methods.

In summary, the MRB-II energy control strategy effectively capitalizes on the simple and practical advantages of the rule-based strategy while integrating an adaptive optimization-seeking kernel, rendering the algorithm both highly efficient and streamlined. By optimizing the characteristic parameters of the power coupling mechanism through the GOP method, we achieve hardware-level optimization that augments vehicle economy. To substantiate the efficacy of this design, comprehensive comparative analyses will be conducted across various road conditions, thereby verifying the improvement in performance.

6. Conclusions

To enhance the fuel economy of the power-split PHEB system, an MRB energy management strategy and a GOP method for optimizing powertrain parameters were proposed, leading to the following conclusions:

1. Innovatively combining rule-based algorithms with intelligent algorithms. Based on the DP algorithm, the optimal working mode point of the power system under any speed and power combination state is solved, and the mode switching lines of ED-PS and PS-ED are designed in combination with the distribution of the working points, which are used as the control rules of ED/OOL to formulate the MRB energy management strategy. The results showed that compared with CDCS, MRB-II reduced fuel consumption by 12.02% and 10.35% under CCBC and synthetic conditions, respectively, and reduced battery life loss by 33.33% and 31.64%, with significant effects.
2. The innovative optimization algorithm for multilayer GOP driveline parameters, aimed at maximizing system efficiency, was constructed. The genetic algorithm is used to generate three parameters of the driveline α_1, α_2, and i_0, which are imported into the designed OAME strategy to adaptively solve the pure electric drive efficiency under the optimal coupling coefficient for single-motor or dual-motor operation modes, and into the PSO algorithm to solve the power generation efficiency under the optimal operating point state of the power generation system in the parking and charging mode. The optimal drive train parameters are obtained by rolling iterations. The PHEB with optimized driveline parameters reduced fuel consumption by 9.04% and 18.11% under CCBC and synthetic conditions, respectively, and by 3.19% and 7.42% at the level of battery life loss, which demonstrates a substantial elevation in the fuel economy and battery protection capabilities of PHEB.
3. The proposed MRB energy management strategy and GOP optimization method for powertrain parameters, balancing both engine fuel economy and overall powertrain efficiency, represent effective approaches for energy management and powertrain optimization in HEVs.

In view of the possible limitations of this article, the next research direction is as follows:

1. At the operational level, the impact indicators of altitude change on power distribution can be added, and the slope parameters can be synthesized by methods such as the Markov chain, so as to construct multi-dimensional conditions based on speed-slope, in order to improve the adaptability of MRB-EMS (MRB-II) in other regions.
2. For the inner switching logic of MRB-II, methods such as machine learning or model prediction can be combined to predict the future speed and speed change to achieve the intelligent switching of modes.

Author Contributions: Conceptualization: L.W. and J.Z. (Juanying Zhou); Methodology: J.Z. (Jianyou Zhao); Software: L.W.; Validation: J.Z. (Juanying Zhou); Formal Analysis: J.Z. (Juanying Zhou); Investigation: L.W.; Resources: J.Z. (Jianyou Zhao); Data Curation: L.W.; Writing—Original Draft Preparation: J.Z. (Juanying Zhou); Writing—Review and Editing: J.Z. (Juanying Zhou); Visualization: L.W.; Supervision: L.W.; Project Administration: J.Z. (Jianyou Zhao); Funding Acquisition: L.W. and J.Z. (Jianyou Zhao). All authors have read and agreed to the published version of the manuscript.

Funding: This research was funded by the National Key Research and Development Program of China, grant number 2020YFB1600400.

Data Availability Statement: The original contributions presented in the study are included in the article, further inquiries can be directed to the corresponding author.

Conflicts of Interest: The authors declare no conflict of interest.

References

1. Chen, X.; Liu, Y.; Wang, Q.; Lv, J.; Wen, J.; Chen, X.; Kang, C.; Cheng, S.; McElroy, M.B. Pathway Toward Carbon-neutral Electrical Systems in China by Mid-century with Negative CO_2 Abatement Costs Informed by High-resolution Modeling. *Joule* **2021**, *5*, 2715–2741. [CrossRef]
2. Zhan, S.; Midgley, W.J.B.; Chen, W.-H.; Steffen, T. An offline closed-form optimal predictive power management strategy for plug-in hybrid electric vehicles. *IEEE Trans. Control. Syst. Technol.* **2022**, *31*, 543–554. [CrossRef]
3. Sakouvogui, A.; Camara, E.O.; Balde, N.A.; Keita, M. Sizing and simulation of a hybrid hydroelectricity and photovoltaic system with storage for supplying the tamagaly district in mamou, guinea. *J. Energy Power Eng.* **2023**, *17*, 69–77.

4. Sulaiman, N.; Hannan, M.; Mohamed, A.; Majlan, E.; Daud, W.W. A Review on Energy Management System for Fuel Cell Hybrid Electric Vehicle: Issues and Challenges. *Renew. Sustain. Energy Rev.* **2015**, *52*, 802–814. [CrossRef]
5. Si, S.; Yang, B.; Gao, B.; Zhang, Z.; Zhao, B.; Zhang, T.; Xu, H. A real-time energy management strategy combining rule and optimization for minimizing energy consumption and emissions of flywheel hybrid electric vehicle (FHEV). *Appl. Thermal Eng.* **2024**, *255*, 124013. [CrossRef]
6. He, H.; Guo, J.; Peng, J.; Tan, H.; Sun, C. Real-time Global Driving Cycle Construction and the Application to Economy Driving Prosystem in Plug-in Hybrid Electric Vehicles. *Energy* **2018**, *150*, 95–107. [CrossRef]
7. Fan, L.; Zhang, Y.; Dou, H.; Zou, R. Design of an Integrated Energy Management Strategy for a Plug-in Hybrid Electric Bus. *J. Power Sources* **2020**, *448*, 227391. [CrossRef]
8. Chai, H.; Zhao, X.; Yu, Q.; Wang, S.; Han, Q.; Zheng, Z. Adaptive equivalent consumption minimization strategy based on road grade estimation for a plug-in hybrid electric truck. *J. Energy Storage* **2023**, *70*, 1.1–1.16. [CrossRef]
9. Liang, G.; Wu, Z.; Didier, C.; Zhang, W.; Cuan, J.; Li, B.; Ko, K.; Hung, P.; Lu, C.; Chen, Y.; et al. A long cycle-life high-voltage spinel lithium-ion battery electrode achieved by site-selective doping. *Angew. Chem. Int. Ed.* **2020**, *59*, 10594–10602. [CrossRef]
10. Pan, W.; Wu, Y.; Tong, Y.; Li, J.; Liu, Y. Optimal rule extraction-based real-time energy management strategy for series-parallel hybrid electric vehicles. *Energy Convers. Manag.* **2023**, *293*, 1.1–1.15. [CrossRef]
11. Liu, X.; Yang, C.; Meng, Y.; Zhu, J.; Duan, Y.; Chen, Y. Hierarchical energy management of plug-in hybrid electric trucks based on state-of-charge optimization. *J. Energy Storage* **2023**, *72*, 107999. [CrossRef]
12. Ruan, J.; Wu, C.; Liang, Z.; Liu, K.; Li, B.; Li, W.; Li, T. The application of machine learning-based energy management strategy in a multi-mode plug-in hybrid electric vehicle, part ii: Deep deterministic policy gradient algorithm design for electric mode. *Energy* **2023**, *269*, 126792. [CrossRef]
13. Aghaei, J.; Nezhad, A.E.; Rabiee, A.; Rahimi, E. Contribution of Plug-in Hybrid Electric Vehicles in Power System Uncertainty Management. *Renew. Sustain. Energy Rev.* **2016**, *59*, 450–458. [CrossRef]
14. Yao, Z.; Yoon, H.S. Hybrid electric vehicle powertrain control based on reinforcement learning. *SAE Int. J. Electrified Veh.* **2022**, *11*, 165–176. [CrossRef]
15. Wang, B.; Zhang, Z.; Xu, Z. Optimal starting control strategy of compound power-split system based on dynamic programing algorithm. *Proc. Inst. Mech. Eng. Part D J. Automob. Eng.* **2023**, *237*, 2580–2591. [CrossRef]
16. Wang, X.; Wang, Q. Application of dynamic programming algorithm based on model predictive control in hybrid electric vehicle control strategy. *Internet Things* **2020**, *2*, 7. [CrossRef]
17. Zeng, X.H.; Wang, Z.W.; Song, D.F. Parameter Optimization of Dual-Mode Power-Split Hybrid Electric Bus Based on MIGA Algorithm. *J. Mech. Eng.* **2020**, *56*, 98–105.
18. Jiang, J.L. *Matching Simulation Study of Plug-In Coaxial Parallel Hybrid Powertrain*; Yanshan University: Qinhuangdao, China, 2014.
19. Lei, N.; Zhang, H.; Wang, H.; Wang, Z. An improved co-optimization of component sizing and energy management for hybrid powertrains interacting with high-fidelity model. *IEEE Trans. Veh. Technol.* **2023**, *72*, 15585–15596. [CrossRef]
20. Xue, Q.; Zhang, X.; Chen, H.; Yue, M.; Teng, T.; Yu, J. Dynamic coordinated control strategy of a dual-motor hybrid electric vehicle based on clutch friction torque observer. *Heliyon* **2024**, *10*, e27255. [CrossRef]
21. Aslan, S.; Karaboga, D. A genetic artificial bee colony algorithm for signal reconstruction based big data optimization. *Appl. Soft Comput.* **2020**, *88*, 106053. [CrossRef]
22. Drallmeier, J.A.; Nazari, S.; Solbrig, R.S.J. Intelligent setpoint optimization for a range extender hybrid electric vehicle with opposed piston engine. *J. Dyn. Syst. Meas. Control.* **2024**, *146*, 1–14. [CrossRef]
23. Quan, R.; Wang, C.; Wu, F.; Chang, Y.; Deng, Y. Parameter matching and optimization of an isg mild hybrid powertrain based on an automobile exhaust thermoelectric generator. *J. Electron. Mater.* **2020**, *49*, 2734–2746. [CrossRef]
24. Zhou, J.Y.; Wang, L.F.; Wang, L.; Zhao, J.Y. Adaptive energy management strategy of plug-in hybrid electric bus. *Comput. Electr. Eng.* **2023**, *112*, 108983. [CrossRef]
25. DB31T 306-2020 General Technical Requirements for Public City Bus [DB/OL]. Instrument Information Network. Available online: https://www.instrument.com.cn/download/shtml/1158272.shtml (accessed on 6 May 2023).